ACS APPLIED MATERIALS & INTERFACES

Letter

www.acsami.org

Large Planar π-Conjugated Porphyrin for Interfacial Engineering in p-i-n Perovskite Solar Cells

Bobo Li,[†] Chaoyue Zheng,[†] Huan Liu,[‡] Jie Zhu,[†] Hongmei Zhang,*[,‡] Deqing Gao,*[,†] and Wei Huang*[,†,‡]

[†]Key Laboratory of Flexible Electronics (KLOFE) & Institute of Advanced Materials (IAM), Jiangsu National Synergistic Innovation Centre for Advanced Materials (SICAM), Nanjing Tech University (NanjingTech), 30 South Puzhu Road, Nanjing 211816, P.R. China

[‡]Key Laboratory for Organic Electronics and Information Displays (KLOEID), Institute of Advanced Materials (IAM), Jiangsu National Synergetic Innovation Center for Advanced Materials (SICAM), Nanjing University of Posts & Telecommunications, 9 Wenyuan Road, Nanjing 210023, P.R. China

Supporting Information

ABSTRACT: In hybrid organic−inorganic perovskite solar cells (PSCs), interfacial engineering can efficiently improve the photovoltaic performance. In this work, the planar π-conjugated porphyrin, zinc(II) 5,10,15,20-tetrakis[5-(p-acetylthiopentyloxy)phenyl]-porphyrin, was developed to modify the interface between poly(3,4-ethylenedioxythiophene):poly(styrenesulfonic acid) (PEDOT:PSS) and perovskite. The modified devices increased their highest power conversion efficiency (PCE) to 14.05% relative to 11.35% for the reference devices without modification. Such enhancement in efficiency is mainly attributed to the improved open-circuit voltage (V_{oc}) and fill factor (FF), which benefit from fast hole-extraction and low charge recombination after the employment of well-aligned interlayer.

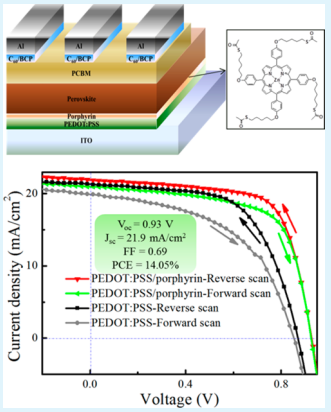

KEYWORDS: *perovskite solar cell, porphyrin, interfacial modification, hole extraction, charge recombination*

The novel and efficient solar cell based on hybrid organometal halide perovskite (AMX_3, A = $CH_3NH_3^+$, $HC(NH_2)_2^+$; M = Pb^{2+}, Sn^{2+}; X = Cl^-, Br^-, I^-) has attracted tremendous attention since it was pioneered by Miyasaka and co-workers in 2009.[1] The perovskite materials exhibit excellent optoelectronic properties, such as high light-absorption coefficient, long exciton diffusion length, and charge carrier lifetime, tunable optical band gap and low exciton binding energy.[2−6] Additionally, the merits of low-cost and solution processability make perovskite semiconductors promising in the commercial application. In the past several years, the highest efficiency of perovskite solar cells has been rapidly increased from an initial 3.8% to a certified 22.1%,[1,7] which is mainly attributed to the improvement of film fabrication techniques and device architecture.

Two representative types of perovskite devices, including conventional electron transfer layer (ETL, such as TiO_2)/perovskite/hole transfer layer (HTL, such as spiro-OMeTAD) (n-i-p) and inverted HTL (such as PEDOT:PSS)/perovskite/ETL (such as PCBM) (p-i-n), are mostly reported.[8−12] Although the former is easy to achieve higher efficiency, the high temperature (T > 400 °C) for fabricating TiO_2 limits the widespread application of the technology and the development of flexible PSCs. Instead, the inverted architecture usually employs low-temperature processed charge-transport layers and avoids the use of mesoporous layer, thus simplifying the fabrication process and reducing the cost. In PSCs, the efficiency loss usually originates from the charge recombination at grain boundaries in the perovskite film and imperfect interfaces of the device. As previously reported, appropriate interfacial engineering can not only promote the charge transport and retard the carrier recombination, but also tune the film morphology through controlling the perovskite crystal growth. Early, p-type poly-TPD was spin-coated onto PEDOT:PSS layer which acted as the electron-blocking layer.[13] Later, Meredith and co-workers have introduced different p-type semiconductors, such as poly(*N*-9′-heptadecanyl-2,7-carbazole-*alt*-5,5-(4′,7′-di(thien-2-yl)-2′,1′,3′-benzothiadiazole)) (PCDTBT) and poly(3-*n*-hexylthiophene) (P3HT), as interfacial layers between PEDOT:PSS and perovskite layers.[14] Then the potential barrier at the PEDOT:PSS/perovskite interface was lowered, which was due to the adjustment of work function of ITO/PEDOT:PSS after the modification. Similarly, new PTPAFSONa and $PTPADCF_3FSONa$ copolymers were inserted between PEDOT:PSS and perovskite, leading to the reduced interfacial

Received: August 17, 2016
Accepted: October 4, 2016

DOI: 10.1021/acsami.6b10342
ACS Appl. Mater. Interfaces XXXX, XXX, XXX−XXX

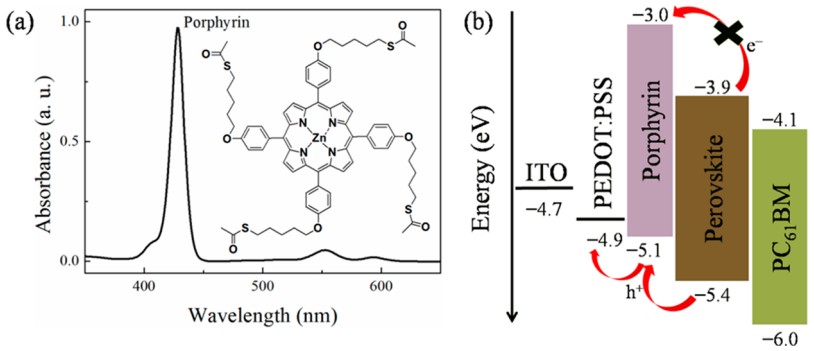

Figure 1. (a) Optical absorption spectrum (measured in *o*-DCB solution with concentration of 1×10^{-6} M) and the molecular structure (inset) of porphyrin. (b) Energy level diagram of each layer.

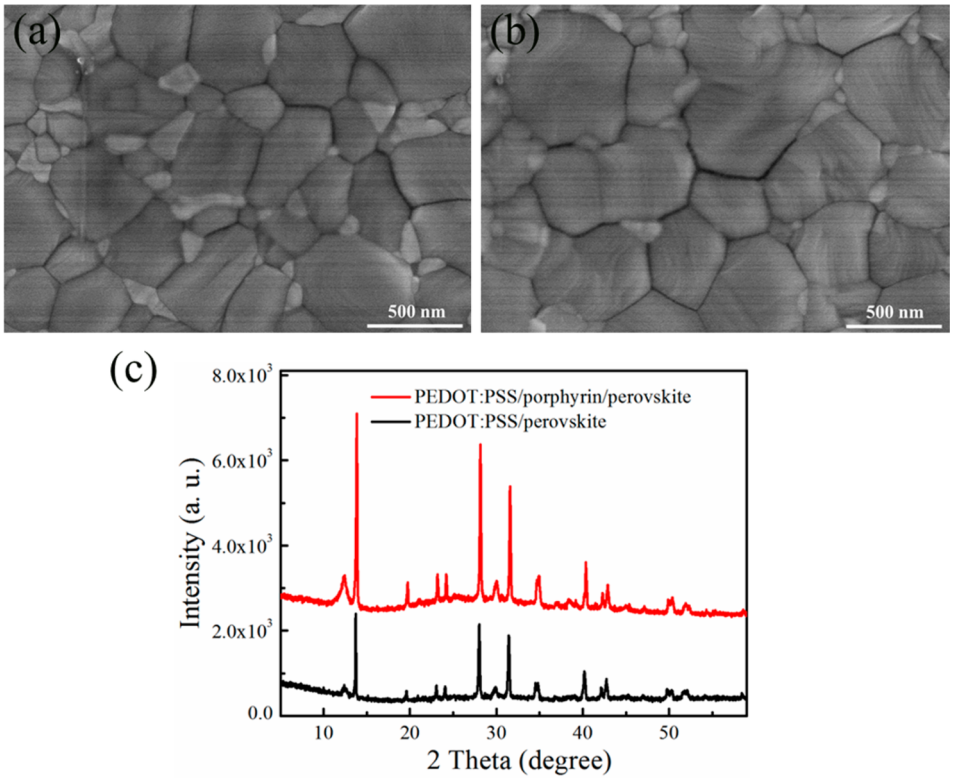

Figure 2. Top-view SEM images of perovskite films on (a) PEDOT:PSS and (b) PEDOT:PSS/porphyrin substrates; (c) XRD patterns of perovskite films grown on different substrates.

trap-assisted recombination.[15] Liao et al. spin-coated a perylene ($C_{20}H_{12}$) interlayer between PEDOT:PSS and perovskite which was beneficial for perovskite growth, tailoring energy-level and reducing trap densities.[16] In addition, Chen et al. modified the interface of PEDOT:PSS/perovskite by utilizing the 3-amino-propanoic self-assembled monolayer. With modification, the perovskite surface morphology was improved, resulting in better device performance and stability.[17] In conventional n-i-p structure, Li et al. also have introduced an F4TCNQ layer at the interface of PEDOT:PSS/HTL through spin-coating from its saturated solution, which resulted in surface passivation and low carrier recombination.[18]

As is well-known, porphyrins are heterocyclic macrocycles with large planar π-conjugation, strong light absorption, unique electronic and magnetic properties, and superior chemical stability. Moreover, porphyrin molecules have abundant functional sites at the periphery of macrocycle, thus their photoelectric properties can be tuned through synthetical modification or substituents.[19,20] Up to now, porphyrin has been widely used as donor material, interlayer, or light-absorbing dye in the field of organic photovoltaic and dye-sensitized solar cell.[21−23] Nevertheless, to the best of our knowledge, porphyrin has not been applied in PSCs yet. Herein, we report here the implementation of p-type porphyrin derivative, zinc(II) 5,10,15,20-tetrakis[5-(p-acetylthiopentyl-oxy)phenyl]porphyrin, as the ultrathin interlayer between PEDOT:PSS and perovskite layers through spin-coating from a 1,2-dichlorobenzene (*o*-DCB) solution. The $-SCOCH_3$ groups (-SAc) in porphyrin molecules can be chemically absorbed onto PEDOT:PSS molecules through electrostatic interaction. The perovskite film formed on porphyrin-modified substrate exhibits large-sized crystals due to the decreased number of nucleation sites on the nonwetting surface of PEDOT:PSS/porphyrin. The matched interfacial energy level

DOI: 10.1021/acsami.6b10342
ACS Appl. Mater. Interfaces XXXX, XXX, XXX−XXX

alignment can facilitate the hole-extraction and reduce the charge recombination. Finally, the V_{oc} and FF of the PSC based on porphyrin are dramatically enhanced, resulting in a best efficiency of 14.05%, which is about 24% higher than the device without modification.

The porphyrin derivative, zinc(II) 5,10,15,20-tetrakis[5-(p-acetylthiopentyloxy)phenyl]porphyrin, was synthesized in our laboratory. The UV−vis light absorption spectrum and molecular structure (inset) of porphyrin are shown in Figure 1a. The spectrum exhibits a sharp Soret band at 428 nm, while two weak Q bands appear at 553 and 595 nm. In addition, the electrochemical properties measured through cyclic voltammetry (CV) are shown in Figure S1. The highest occupied molecular orbital (HOMO) and lowest unoccupied molecular orbital (LUMO) levels of −5.1 eV and −3.0 eV can be calculated from the following equations: (a) HOMO = −(4.4 + E_{ox}) and (b) LUMO = HOMO+1240/λ_{cutoff}.[24] The values of E_{ox} and λ_{cutoff} were determined from UV−vis and CV spectra, respectively. Figure 1b depicts the corresponding energy level diagram. We can see that the LUMO of porphyrin is higher than the conduction band edge of perovskite (−3.9 eV, versus vacuum),[25] indicating that electron-transport barrier exists in these two layers, thus retarding the carrier recombination at the PEDOT:PSS/perovskite interface. Meanwhile, the higher HUMO energy level of porphyrin relative to perovskite (−5.4 eV, versus vacuum) can efficiently facilitate hole extraction and transport.

The porphyrin interlayers were introduced onto PEDOT:PSS substrates via simple spin-coating method from a *o*-DCB solution (0.5 mg/mL) and all perovskite films on PEDOT:PSS and PEDOT:PSS/porphyrin were fabricated in a similar way as we previously reported.[26] We first compared the light absorption of porphyrin film before and after spin-coating N,N-dimethylformamide (DMF) solvent in order to test the intersolubility between porphyrin and perovskite films. The spectra are shown in Figure S2 and we can see that the change was almost negligible, indicating that the porphyrin film exhibited good resistance against DMF. Subsequently, the surface morphology of porphyrin layer was investigated by using atomic force microscope (AFM) (as presented in Figure S3). It can be seen that a compact layer of porphyrin covers the entire area of the PEDOT:PSS and some aggregates are uniformly distributed on the surface. This is in agreement with the reported observation previously.[23]

Then to understand the influence of porphyrin on the perovskite crystals growth, the characterization of the top-view scanning electron microscope (SEM) was implemented. Figures 2a and 2b exhibit the evolution in surface morphology of perovskite films formed on different substrates. It is clear that the perovskite crystals grown on bare PEDOT:PSS exhibits a distribution in the range of 50−700 nm size and an average size of 296 nm (Figure S4). However, the largest and average crystal sizes of the comparative perovskite film fabricated on modified PEDOT:PSS increase up to 1 μm and 530 nm, respectively. In our experiments, we observed that the droplets of PbI_2 precursor solution were hard to freely spread on porphyrin-modified substrate. The experimental phenomenon was recorded in Figure S5. We dropped the same amount of PbI_2 (20 μL) solution onto the ITO/PEDOT:PSS and ITO/PEDOT:PSS/porphyrin substrates and then took photographs after 3 and 10 s, respectively. Herein, we speculate that the large crystal sizes are mainly attributed to the nonwetting surface of PEDOT:PSS/porphyrin, thus resulting in the decrease of the number of nucleation sites. This result is consistent with the perovskite films formed on hydrophobic HTLs reported by Huang's group.[27] As the carrier recombination is often caused by the trap sites at the grain boundaries,[27−29] the large-sized crystals indicate that the charge recombination and loss in the bulk perovskites film on PEDOT:PSS/porphyrin can be restrained to some extent. Furthermore, we studied the crystallinity of the perovskite films grown on different substrates through X-ray diffraction (XRD) measurement. As shown in Figure 2c, although these two films exhibited three main peaks at around 14, 28, and 32°, the film formed on modified substrate exhibited higher peak intensity than that formed on bare PEDOT:PSS substrate. This result further indicated that the insertion of porphyrin interlayer can favor the crystallization of perovskite film.

Next, to further investigate the effect of porphyrin on the hole extraction and transport at the PEDOT:PSS/perovskite interface, we performed photoluminescence (PL) measurements of perovskite films on ITO/PEDOT:PSS and ITO/PEDOT:PSS/porphyrin to study the charge dynamics. Both of these two perovskite films exhibit a similar emission peak at around 775 nm in the steady-state PL spectra, as shown in Figure 3a. However, the PL intensity of perovskite on modified

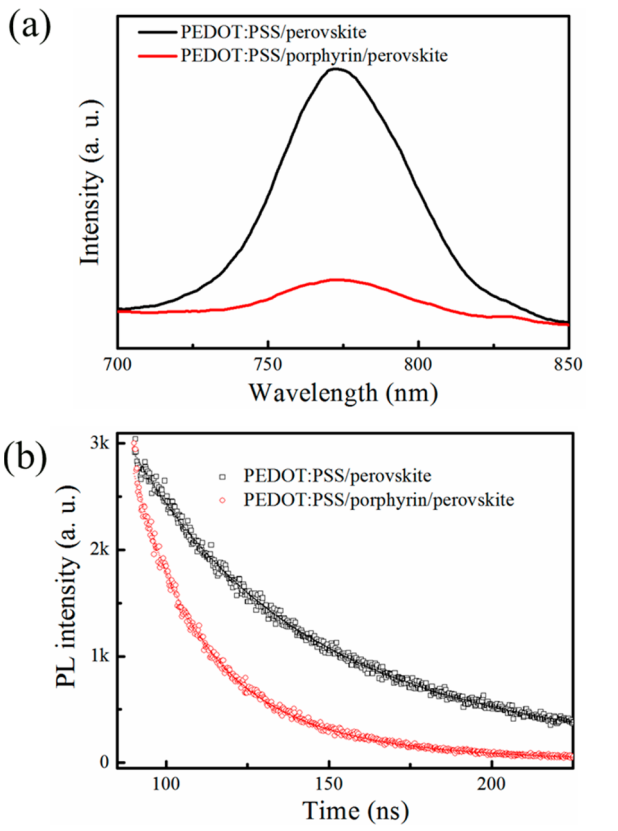

Figure 3. (a) Steady-state and (b) time-resolved photoluminescence spectra of PEDOT:PSS/perovskite and PEDOT:PSS/porphyrin/perovskite films on ITO substrates.

substrate was seriously quenched. This striking quenching phenomenon suggests that porphyrin can act as an effective interlayer for reducing the carrier recombination between HTL and perovskite. Additionally, the time-resolved PL (TR-PL) decay transient curves excited with a 485 nm laser are exhibited in Figure 3b. The spectra represent the signals collected at the

DOI: 10.1021/acsami.6b10342
ACS Appl. Mater. Interfaces XXXX, XXX, XXX−XXX

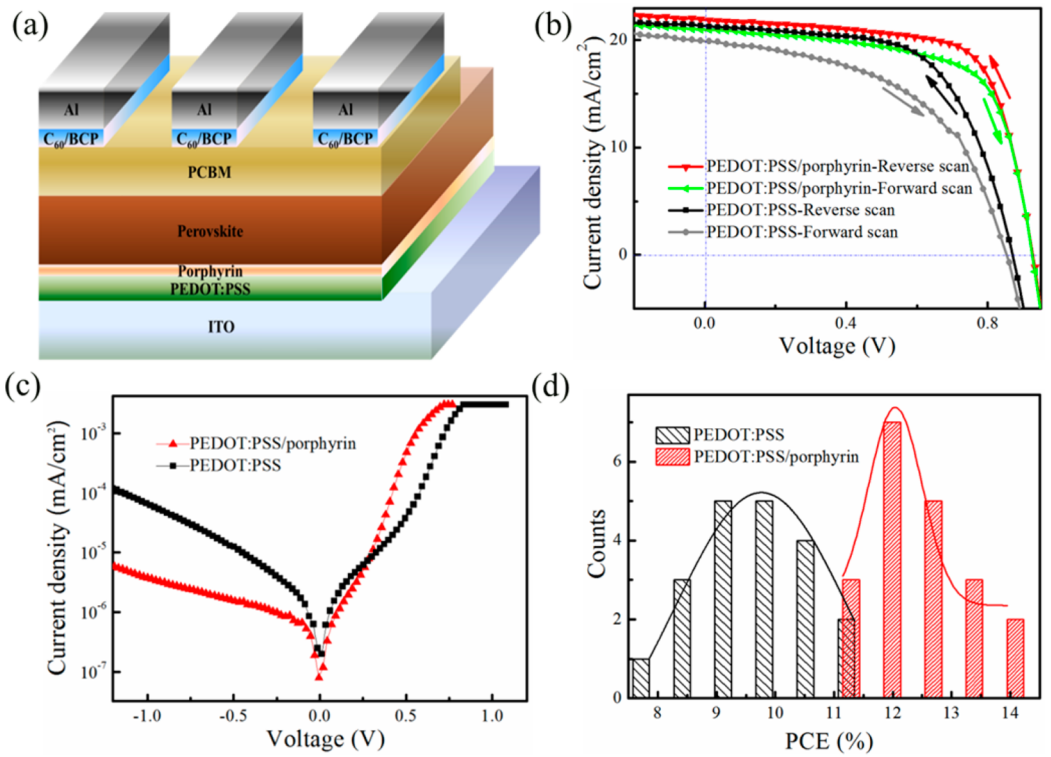

Figure 4. (a) Schematic of the device architecture. Characteristics of perovskite solar cells based on bare PEDOT:PSS and PEDOT:PSS/porphyrin (the 0.5 mg/mL sample): (b) photocurrent density−voltage curves of the optimal devices with reverse and forward scan directions under AM 1.5G simulated sunlight; (c) $J-V$ curves measured in the dark condition with reverse scan direction; (d) power conversion efficiency (under reverse scan) histograms.

wavelength of 775 nm and the lifetime of charge carriers can be calculated by fitting the data. The average lifetime of ITO/PEDOT:PSS/perovskite is 63.9 ns, whereas the corresponding value is shorten to 27.1 ns for the porphyrin-modified sample. This result can further indicate that the introduce of porphyrin can promote hole extraction and transfer from perovskite to PEDOT:PSS at the PEDOT:PSS/perovskite interface.

Then we fabricated the planar perovskite solar cells with active areas of 0.09 cm^2 and the device architecture of ITO/PEDOT:PSS/porphyrin/perovskite/PCBM/C_{60}/BCP/Al is illustrated in Figure 4a. The photovoltaic performances of the devices were measured under AM 1.5G simulated sunlight irradiation (100 mW cm^{-2}) in the ambient condition. Figure 4b gives the light photocurrent−voltage ($J-V$) curves of the optimal devices with and without porphyrin and the corresponding parameters are summarized in Table 1. As we can see, under reverse scan mode, the best device based on bare PEDOT:PSS exhibits an open-circuit voltage of 0.87 V, a short-circuit current density (J_{sc}) of 21.29 mA cm^{-2} and a fill factor of 0.61, yielding a PCE of 11.35%. By contrast, after embedding the porphyrin in the device, a higher efficiency of 14.05% is obtained with a V_{oc} of 0.93 V, a J_{sc} of 21.90 mA cm^{-2} and a FF of 0.69. Note that the improved efficiency is mainly attributed to the increase of V_{oc} and FF. Because it has been reported that the scanning direction has a significant effect on the efficiency, we tested our devices through forward scan. We can see that the $J-V$ hysteresis in porphyrin-modified device was also moderately decreased.

Table 1. Photovoltaic Parameters of the Optimal Perovskite Devices with and without Porphyrin

substrate	sweep direction	V_{oc} (V)	J_{sc} (mA/cm^2)	FF	PCE (%)
PEDOT:PSS	forward	0.85	19.86	0.51	8.71
	reverse	0.87	21.29	0.61	11.35
PEDOT:PSS/porphyrin	forward	0.93	20.98	0.66	12.88
	reverse	0.93	21.90	0.69	14.05

To get an insight in the underlying mechanism influencing the performance of the different PSCs, the electrical behavior of the devices were measured in the dark. As seen in Figure 4c, the dark current density of the device based on PEDOT:PSS/porphyrin under reverse bias (1.2 V to −1.2 V) is about 1×10^{-5} mA cm^{-2}, which is about 1 order of magnitude lower than the pristine one ($\approx 1 \times 10^{-4}$ mA cm^{-2}). This indicates that the current leakage is dramatically prevented after interfacial modification. Certainly, the smaller current leakage is ascribed to the lower charge recombination in the modified device. Then we can further explain why the V_{oc} increased in the porphyrin-based device. It is because that V_{oc} is determined by the formula of $V_{oc} = (mRT/F) \ln(I_{sc}/I_0 - 1)$, where I_{sc} represents the short-circuit current, I_0 is the dark current, and m, R, and F represent ideality factor, idea gas, and Faraday constants, respectively.[30] So lower I_0 means higher V_{oc}. In addition, the enhancement in FF was due to the good interfacial compatibility at the perovskite/PEDOT:PSS interface and efficient hole extraction and transport through inserting a porphyrin interlayer. The changes in V_{oc} and FF are in good agreement with the variations in surface morphology, photoluminescence intensity, and charge lifetime.

Moreover, we also changed the concentration of porphyrin solution and measured the influence of the interlayer's thickness on the device performance. It can be found that all

DOI: 10.1021/acsami.6b10342
ACS Appl. Mater. Interfaces XXXX, XXX, XXX−XXX

the devices with porphyrin have higher efficiency than that without interlayer, as shown in Figure S6 and Table S1. The efficiency difference for porphyrin-modified solar cells is less than 0.7% when the concentration of porphyrin solution is varying from 0.25 to 2 mg/mL (in *o*-DCB solution). Further investigation on the thickness and corresponding mechanism will be performed in detail in the future.

Finally, the PCE histograms of 20 individual devices (the 0.5 mg/mL sample) and the corresponding standard errors are summarized in Figure 4d and Table S2, respectively. In addition, distributions of J_{sc}, V_{oc}, and FF are presented in Figure S7. All these efficiency were obtained through scanning from positive to negative bias. The porphyrin-based PSCs exhibited excellent reproducibility and most of the devices have PCE higher than 11.0%.

In conclusion, we have demonstrated that the employment of large planar π-conjugated porphyrin at the PEDOT:PSS/perovskite interface is effective in improving the photovoltaic performance of perovskite solar cells. The porphyrin can facilitate the formation of perovskite film with large-sized crystals, high crystallinity, and low traps. Additionally, the well-aligned energy level among the PEDOT:PSS, porphyrin and perovskite can efficiently promote the hole extraction and reduce the charge recombination and loss, which are intuitively reflected in the shortened lifetime and quenched photoluminescence intensity. As a result, a high efficiency of 14.05% has been achieved for the device based on PEDPT:PSS/porphyrin, which was mainly attributed to the increase of V_{oc} and FF. Therefore, our work proved that the interlayer based on the planar π-conjugated porphyrin is a promising candidate in perovskite solar cells.

■ ASSOCIATED CONTENT

Supporting Information

The Supporting Information is available free of charge on the ACS Publications website at DOI: 10.1021/acsami.6b10342.

Detailed experimental procedures, AFM of porphyrin layer, $J-V$ curves of the devices with different concentrations of porphyrin solution, the device parameter distributions (V_{oc}, J_{sc}, and FF) and other characterizations (PDF)

■ AUTHOR INFORMATION

Corresponding Authors

*E-mail: iamdqgao@njtech.edu.cn.
*E-mail: iamhmzhang@njupt.edu.cn.
*E-mail: iamwhuang@njtech.edu.cn.

Notes

The authors declare no competing financial interest.

■ ACKNOWLEDGMENTS

This work was supported by National Key Basic Research Program of China under Grant 2015CB932200 (D.G. and W.H.).

■ REFERENCES

(1) Kojima, A.; Teshima, K.; Shirai, Y.; Miyasaka, T. Organometal Halide Perovskites as Visible-Light Sensitizers for Photovoltaic Cells. *J. Am. Chem. Soc.* **2009**, *131*, 6050−6051.

(2) Etgar, L.; Gao, P.; Xue, Z.; Peng, Q.; Chandiran, A. K.; Liu, B.; Nazeeruddin, M. K.; Grätzel, M. Mesoscopic $CH_3NH_3PbI_3/TiO_2$ Heterojunction Solar Cells. *J. Am. Chem. Soc.* **2012**, *134*, 17396−17399.

(3) Stranks, S. D.; Eperon, G. E.; Grancini, G.; Menelaou, C.; Alcocer, M. J.; Leijtens, T.; Herz, L. M.; Petrozza, A.; Snaith, H. J. Electron-Hole Diffusion Lengths Exceeding 1 Micrometer in an Organometal Trihalide Perovskite Absorber. *Science* **2013**, *342*, 341−344.

(4) Xing, G.; Mathews, N.; Sun, S.; Lim, S. S.; Lam, Y. M.; Grätzel, M.; Mhaisalkar, S.; Sum, T. C. Long-Range Balanced Electron- and Hole-Transport Lengths in Organic-Inorganic $CH_3NH_3PbI_3$. *Science* **2013**, *342*, 344−347.

(5) Noh, J. H.; Im, S. H.; Heo, J. H.; Mandal, T. N.; Seok, S. I. Chemical Management for Colorful, Efficient, and Stable Inorganic-Organic Hybrid Nanostructured Solar Cells. *Nano Lett.* **2013**, *13*, 1764−1769.

(6) Xu, X.; Liu, Z.; Zuo, Z.; Zhang, M.; Zhao, Z.; Shen, Y.; Zhou, H.; Chen, Q.; Yang, Y.; Wang, M. Hole Selective NiO Contact for Efficient Perovskite Solar Cells with Carbon Electrode. *Nano Lett.* **2015**, *15*, 2402−2408.

(7) http://www.nrel.gov/ncpv/images/efficiency_chart.jpg.

(8) Burschka, J.; Pellet, N.; Moon, S. J.; Humphry-Baker, R.; Gao, P.; Nazeeruddin, M. K.; Grätzel, M. Sequential Deposition as a Route to High-Performance Perovskite-Sensitized Solar Cells. *Nature* **2013**, *499*, 316−319.

(9) Lee, M. M.; Teuscher, J.; Miyasaka, T.; Murakami, T. N.; Snaith, H. J. Efficient Hybrid Solar Cells Based on Meso-Superstructured Organometal Halide Perovskites. *Science* **2012**, *338*, 643−647.

(10) Bi, D.; El-Zohry, A. M.; Hagfeldt, A.; Boschloo, G. Improved Morphology Control Using a Modified Two-Step Method for Efficient Perovskite Solar Cells. *ACS Appl. Mater. Interfaces* **2014**, *6*, 18751−18757.

(11) You, J.; Hong, Z.; Yang, Y. M.; Chen, Q.; Cai, M.; Song, T.-B.; Chen, C.-C.; Lu, S.; Liu, Y.; Zhou, H.; Yang, Y. Low-Temperature Solution-Processed Perovskite Solar Cells with High Efficiency and Flexibility. *ACS Nano* **2014**, *8*, 1674−1680.

(12) Li, X.; Liu, X.; Wang, X.; Zhao, L.; Jiu, T.; Fang, J. Polyelectrolyte Based Hole-Transporting Materials for High Performance Solution Processed Planar Perovskite Solar Cells. *J. Mater. Chem. A* **2015**, *3*, 15024−15029.

(13) Malinkiewicz, O.; Yella, A.; Lee, Y. H.; Espallargas, G. M. n.; Graetzel, M.; Nazeeruddin, M. K.; Bolink, H. J. Perovskite Solar Cells Employing Organic Charge-Transport Layers. *Nat. Photonics* **2014**, *8*, 128−132.

(14) Lin, Q.; Armin, A.; Nagiri, R. C. R.; Burn, P. L.; Meredith, P. Electro-Optics of Perovskite Solar Cells. *Nat. Photonics* **2015**, *9*, 106−112.

(15) Xue, Q.; Chen, G.; Liu, M.; Xiao, J.; Chen, Z.; Hu, Z.; Jiang, X.-F.; Zhang, B.; Huang, F.; Yang, W.; Yip, H.-L.; Cao, Y. Improving Film Formation and Photovoltage of Highly Efficient Inverted-Type Perovskite Solar Cells Through the Incorporation of New Polymeric Hole Selective Layers. *Adv. Energy Mater.* **2016**, *6*, 1502021.

(16) Wang, Z. K.; Gong, X.; Li, M.; Hu, Y.; Wang, J. M.; Ma, H.; Liao, L. S. Induced Crystallization of Perovskites by a Perylene Underlayer for High-Performance Solar Cells. *ACS Nano* **2016**, *10*, 5479−5489.

(17) Gu, Z.; Zuo, L.; Larsen-Olsen, T. T.; Ye, T.; Wu, G.; Krebs, F. C.; Chen, H. Interfacial Engineering of Self-Assembled Monolayer Modified Semi-Roll-to-Roll Planar Heterojunction Perovskite Solar Cells on Flexible Substrates. *J. Mater. Chem. A* **2015**, *3*, 24254−24260.

(18) Song, D.; Wei, D.; Cui, P.; Li, M.; Duan, Z.; Wang, T.; Ji, J.; Li, Y.; Mbengue, J. M.; Li, Y.; He, Y.; Trevor, M.; Park, N.-G. Dual Function Interfacial Layer for Highly Efficient and Stable Lead Halide Perovskite Solar Cells. *J. Mater. Chem. A* **2016**, *4*, 6091−6097.

(19) Ishihara, S.; Labuta, J.; Van Rossom, W.; Ishikawa, D.; Minami, K.; Hill, J. P.; Ariga, K. Porphyrin-Based Sensor Nanoarchitectonics in Diverse Physical Detection Modes. *Phys. Chem. Chem. Phys.* **2014**, *16*, 9713−9746.

(20) Li, L. L.; Diau, E. W. Porphyrin-Sensitized Solar Cells. *Chem. Soc. Rev.* **2013**, *42*, 291−304.

DOI: 10.1021/acsami.6b10342
ACS Appl. Mater. Interfaces XXXX, XXX, XXX−XXX

(21) Shao, Y.; Yang, Y. Efficient Organic Heterojunction Photovoltaic Cells Based on Triplet Materials. *Adv. Mater.* **2005**, *17*, 2841−2844.
(22) Mathew, S.; Yella, A.; Gao, P.; Humphry-Baker, R.; Curchod, B. F. E.; Ashari-Astani, N.; Tavernelli, I.; Rothlisberger, U.; Nazeeruddin, M. K.; Grätzel, M. Dye-Sensitized Solar Cells with 13% Efficiency Achieved Through the Molecular Engineering of Porphyrin Sensitizers. *Nat. Chem.* **2014**, *6*, 242−247.
(23) Vasilopoulou, M.; Georgiadou, D. G.; Douvas, A. M.; Soultati, A.; Constantoudis, V.; Davazoglou, D.; Gardelis, S.; Palilis, L. C.; Fakis, M.; Kennou, S.; Lazarides, T.; Coutsolelos, A. G.; Argitis, P. Porphyrin Oriented Self-Assembled Nanostructures for Efficient Exciton Dissociation in High-Performing Organic Photovoltaics. *J. Mater. Chem. A* **2014**, *2*, 182−192.
(24) Gong, X. J.; Xie, X.; Chen, N. W.; Zheng, C. Y.; Zhu, J.; Chen, R. F.; Huang, W.; Gao, D. Q. Two Symmetrically Bis-Substituted Pyrene Derivatives: Synthesis, Photoluminescence, and Electroluminescence. *Chin. J. Chem.* **2015**, *33*, 967−973.
(25) Lim, K.-G.; Kim, H.-B.; Jeong, J.; Kim, H.; Kim, J. Y.; Lee, T.-W. Boosting the Power Conversion Efficiency of Perovskite Solar Cells Using Self-Organized Polymeric Hole Extraction Layers with High Work Function. *Adv. Mater.* **2014**, *26*, 6461−6466.
(26) Chen, Y. N.; Li, B. B.; Huang, W.; Gao, D. Q.; Liang, Z. Q. Efficient and Reproducible $CH_3NH_3PbI_{3-x}(SCN)_x$ Perovskite Based Planar Solar Cells. *Chem. Commun.* **2015**, *51*, 11997−11999.
(27) Bi, C.; Wang, Q.; Shao, Y.; Yuan, Y.; Xiao, Z.; Huang, J. Non-Wetting Surface-Driven High-Aspect-Ratio Crystalline Grain Growth for Efficient Hybrid Perovskite Solar Cells. *Nat. Commun.* **2015**, *6*, 7747.
(28) Li, B.; Jiu, T.; Kuang, C.; Ma, S.; Chen, Q.; Li, X.; Fang, J. Chlorobenzene Vapor Assistant Annealing Method for Fabricating High Quality Perovskite Films. *Org. Electron.* **2016**, *34*, 97−103.
(29) Kuang, C.; Tang, G.; Jiu, T.; Yang, H.; Liu, H.; Li, B.; Luo, W.; Li, X.; Zhang, W.; Lu, F.; Fang, J.; Li, Y. Highly Efficient Electron Transport Obtained by Doping PCBM with Graphdiyne in Planar-Heterojunction Perovskite Solar Cells. *Nano Lett.* **2015**, *15*, 2756−2762.
(30) Li, W.; Dong, H.; Guo, X.; Li, N.; Li, J.; Niu, G.; Wang, L. Graphene Oxide as Dual Functional Interface Modifier for Improving Wettability and Retarding Recombination in Hybrid Perovskite Solar Cells. *J. Mater. Chem. A* **2014**, *2*, 20105−20111.

DOI: 10.1021/acsami.6b10342
ACS Appl. Mater. Interfaces XXXX, XXX, XXX−XXX